Bone 137 (2020) 115402

Contents lists available at ScienceDirect

Bone

journal homepage: www.elsevier.com/locate/bone

Full Length Article

Loss of BMP signaling mediated by BMPR1A in osteoblasts leads to differential bone phenotypes in mice depending on anatomical location of the bones

Honghao Zhang[a,1], Yanshuai Zhang[a,1], Masahiko Terajima[b], Genevieve Romanowicz[a], Yangjia Liu[a,c], Maiko Omi[a], Erin Bigelow[d], Danese M. Joiner[d], Erik I. Waldorff[d], Peizhi Zhu[e], Mekhala Raghavan[e], Michelle Lynch[a], Nobuhiro Kamiya[a,f], Rongqing Zhang[c], Karl J. Jepsen[d], Steve Goldstein[d], Michael D. Morris[e], Mitsuo Yamauchi[b], David H. Kohn[a], Yuji Mishina[a,*]

[a] Department of Biologic and Materials Sciences, School of Dentistry, University of Michigan, MI, USA
[b] School of Dentistry, University of North Carolina at Chapel Hill, North Carolina, NC, USA
[c] School of Life Sciences, Tsinghua University, Beijing, China
[d] Department of Orthopaedic Surgery, Michigan Medicine, University of Michigan, MI, USA
[e] Department of Chemistry, College of Literature, Science and the Arts, University of Michigan, MI, USA
[f] Tenri University, Nara, Japan

ARTICLE INFO

Keywords:
BMP receptor type 1A
Osteoblasts
Collagen cross-links
Bone quality
Biomechanical properties

ABSTRACT

Bone morphogenetic protein (BMP) signaling in osteoblasts plays critical roles in skeletal development and bone homeostasis. Our previous studies showed loss of function of BMPR1A, one of the type 1 receptors for BMPs, in osteoblasts results in increased trabecular bone mass in long bones due to an imbalance between bone formation and bone resorption. Decreased bone resorption was associated with an increased mature-to-immature collagen cross-link ratio and mineral-matrix ratios in the trabecular compartments, and increased tissue-level biomechanical properties. Here, we investigated the bone mass, bone composition and biomechanical properties of ribs and spines in the same genetically altered mouse line to compare outcomes by loss of BMPR1A functions in bones from different anatomic sites and developmental origins. Bone mass was significantly increased in both cortical and trabecular compartments of ribs with minimal to modest changes in compositions. While tissue-levels of biomechanical properties were not changed between control and mutant animals, whole bone levels of biomechanical properties were significantly increased in association with increased bone mass in the mutant ribs. For spines, mutant bones showed increased bone mass in both cortical and trabecular compartments with an increase of mineral content. These results emphasize the differential role of BMP signaling in osteoblasts in bones depending on their anatomical locations, functional loading requirements and developmental origin.

1. Introduction

Bone morphogenetic proteins (BMPs) were originally identified as proteins that can induce ectopic bone formation when implanted subcutaneously [1,2]. Functions of BMP signaling have been extensively studied both in vitro and in vivo as regulators of skeletal development and maintenance of bone mass in adults [3,4]. BMP ligands bind and transduce signals through complexes of type I and type II serine/threonine kinase receptors [5,6]. The activated type I receptor subsequently phosphorylates receptor regulated Smads (R-Smads 1, 5, 8) that then bind to Smad4 [7–11]. This complex translocates into the nucleus and regulates the transcription of target genes [10,12]. Based on their osteogenic activities, use of BMP2 and BMP7 in clinical setting has been approved by the FDA, and their impact on spine fusion and fracture healing has been extensively studied for the last decade [13–20].

We previously reported that disruption of *Bmpr1a* that encodes BMP type IA receptor in an osteoblast-specific manner (cKO) resulted in

* Corresponding author at: Department of Biologic and Materials Sciences, School of Dentistry, University of Michigan, 1011 N. University Ave., Ann Arbor, MI 48109, USA.
E-mail address: mishina@umich.edu (Y. Mishina).
[1] Equal contribution.

https://doi.org/10.1016/j.bone.2020.115402
Received 5 March 2020; Received in revised form 14 April 2020; Accepted 28 April 2020
Available online 01 May 2020

increased bone mass, contrary to expectation due to the reduced osteoclastogenesis and bone resorption secondary to the loss of BMP signaling in osteoblasts [21–24]. Similar results are confirmed by other groups using the same approach to disrupt *Bmpr1a* in osteogenic lineage [25,26]. Osteoblast-specific disruption of *Acvr1* that encodes another BMP type I receptor also results in a high bone mass phenotype [27]. Disruption of *Bmpr2* that encodes BMP type II receptor in a limb mesenchymal-specific manner using *Prrx1*-Cre also results in increased bone mass in the proximal tibia [28]. In addition to these genetic approaches, administration of a soluble form of a BMPR1A fusion protein to wild-type mice to reduce BMP signaling activity leads to an increase in bone mass [29]. Taken together, these results indicate that functions of BMP signaling on bone homeostasis are not as simple as what was believed earlier: BMP signaling in osteoblasts is important to regulate osteoclastogenesis and thus disruption of BMP signaling in osteoblasts also impairs osteoclastogenesis thereby altering a balance between bone formation and bone resorption [22–24]. Unlike these predictions from mounting results of culture studies, increased proliferation of osteoblasts is found in the cKO mice, which could also be a reason of higher bone mass in these cKO mice [25,26,28].

A subsequent important question is whether bones with increased bone mass in cKO mice show alterations in compositions and biomechanical properties. We previously reported using femora as a representative of long bones that loss of BMPR1A in the trabecular compartments shows more mature types of collagen crosslinks and mineral-matrix ratios in association with increased tissue-level biomechanical properties (hardness and elastic modulus), but no overt changes in composition or biomechanical properties in the cortical compartments [30]. Due to the reduction in femoral cortical area (cross-sectional area) in the cKO mice with no change in tissue-level biomechanical properties, whole bone strength (whole bone level) is reduced in the cKO femur [30]. An increase in cortical porosity in the cKO bones may contribute to the reduced whole bone strength, which is reversed via treadmill exercise of the cKO mice, restoring the cortical porosity and the whole bone level biomechanical properties [31].

In this study, we put the focus on other type of bones with primary trabecular compartments and different loading requirements such as ribs and vertebrae, to understand impacts of loss of BMPR1A. Ribs belong to flat bones while vertebrae are regarded as irregular shaped bones, and both are developed from the paraxial mesoderm whereas long bones in the limbs form from the lateral plate mesoderm. The rib bones are important to protect many vital organs and provide additional mechanical support to the spine. Rib fractures are the most common non-traumatic factures in the elderly population that can lead to cardiopulmonary insufficiency [32–34]. The spinal column consists with 29 vertebrae in human (excluding 4 bones that are fused to generate coccyx bones) and 30 vertebrae in mice (excluding 28 caudal vertebrae). Vertebral fractures are also common fractures with significant consequences to patient morbidity [35]. Years of studies suggest a strong correlation between bone mineral density and risk factors for fracture [35–37]. In the previous studies, we found increased bone mass in the cKO mice by histologic observations including long bones, ribs and vertebrae [22–24]. We employed the same strategy as in the previous report to generate *Bmpr1a* cKO mice to evaluated the structure, mineral density, properties of collagen and minerals, and biomechanical properties for ribs and vertebrae. Our results underscored the differential role of BMP signaling in osteoblasts in different bones.

2. Materials and methods

2.1. Animals

A transgenic mouse expressing the tamoxifen (TM)-inducible Cre fusion protein Cre-ER™ [22,23] under the control of a 3.2 kb mouse procollagen *a (I)* promoter [38] (*Col1-CreER™*) was generated by pronuclear injection and crossed with floxed *Bmpr1a* mice [39]. These mice were maintained in a 129S6 and C57BL6/J mixed background. TM (150 mg/kg) was gavaged to both males and females twice a week from 16 to 20 weeks of age and tissues were collected at week 22 (n = 15 per group). Results were analyzed by comparing *Bmpr1a* cKO (*Col1-CreER (+);Bmpr1a*$^{fl/fl}$, cKO, hereafter) and littermate controls (*Col1-CreER (−);Bmpr1a*$^{fl/fl}$, control, hereafter) that also received TM. No side effects on bone morphology or body weight were observed using this TM regimen [21,22]. The animal protocol was approved by the Institutional Animal Care and Use Committee at the National Institute of Environmental Health Sciences and the University of Michigan.

2.2. Micro computed tomography (μCT) evaluation – geometric properties

The left 8th ribs (males, n = 14 for controls and n = 15 for cKO, females, n = 15 for controls and cKO) were scanned at the cortical mid-shaft (Mid) and metaphyseal (End) regions, and the trabecular mid-shaft regions (Mid) using a μCT system (μCT100 Scanco Medical, Bassersdorf, Switzerland). The femoral mid-shaft regions were also scanned from the same mice for comparison. A 0.3 mm region of cortical bone was analyzed beginning 0.5 mm from the growth plate (End region, closer to sternum) using a fixed global threshold of 25.5% (255 on a grayscale of 0–1000); and a 0.4 mm region of cortical bone located around the mid-diaphysis (cortical Mid region) were analyzed using a fixed global threshold of 28% (280 on a grayscale of 0–1000). A 1 mm × 1 mm region of the trabecular compartment was analyzed beginning 0.2 mm from the growth plate (trabecular End region). Scan settings were voxel size 10 μm, voltage 70 kV, current μA, 0.5 mm aluminum filter, and integration time 500 ms. Analysis was performed using the manufacturer's evaluation software.

For vertebrae, the 4th lumbar vertebrae (L4) was dissected, cleaned off soft tissue, stored in phosphate buffered saline (PBS) solution, and frozen until further processing. Specimens were scanned by a cone beam μCT system (GE Healthcare PCI, London, ON), and reconstructed at a voxel size of 18 μm. The cortical region of interest (ROI) tool was used to select the outer shell of the vertebral body for tissue mineral density, thickness, bone mineral density, and cross sectional area calculations. Distal and proximal cylindrical ROIs equal to 15% of the total height of the specimens, comprising trabecular bone within the inner vertebral body, were created to analyze mineralization and trabecular bone architecture. Data collected from the two cylindrical ROIs were averaged to yield one value for each parameter of interest per specimen.

2.3. Amino acid analysis

The 6th ribs (male, n = 3 each group) from left and right were removed at week 22 and soft tissues were cleaned off the bone surface. Bone marrow was removed by flushing with cold PBS and then the samples from each side were combined and pulverized to a fine powder under liquid N2 using a Spex Freezer Mill (Spex Metuchen, NJ, USA). Pulverized samples were washed with cold PBS and then with cold distilled water several times by repeated centrifugation (4000*g*), and lyophilized. One milligram of dried sample was hydrolyzed with 6 N HCl and an aliquot of hydrolysate was subjected to amino acid analysis on a Varian high performance liquid chromatography system (Prostar 240/310, Varian, Walnut Creek, CA, USA) with a strong cation exchange column (AA-911, Transgenomic, San Jose, CA, USA) [40]. Collagen composition (% in total proteins) was calculated as hydroxyproline (Hyp)/1000 total amino acids X 100. Collagen content was calculated as μg/mg of dried sample and the extent of Lys hydroxylation of collagen was calculated by the hydroxylysine (Hyl) residues per 300 residues of Hyp and expressed as mol/mol of collagen [41]. Similarly, the 6th ribs (male, n = 5 each group) from both sides were prepared from of 10 weeks old mice that received TM (150 mg/kg) through gavage twice a week from 5 to 8 weeks of age and tissues were collected at week 10 for amino acid analysis and subsequent cross-link analysis. Ribs from each side were analyzed separately in this group.

2.4. Collagen cross-link analysis

Ribs were demineralized with 0.5 M EDTA, 0.05 M of Tris-HCl, pH 7.4, for 2 weeks, and washed with cold distilled water exhaustively and lyophilized. Two milligrams of demineralized bone was then suspended, and hydrolyzed with 6 N HCl as described above. An aliquot of hydrolysate was subjected to amino acid analysis to determine Hyp and then the hydrolysate with known amounts of Hyp was analyzed for cross-linking on a Varian HPLC system (with AA911 column, see above) linked to an on-line fluorescence flow monitor (FP-1520, Jasco, Tokyo, Japan) and a liquid scintillation flow monitor (500TR series, Packard Instrument, Meriden, CT, USA). The non-reducible cross-links, Hydroxylysyl Pyridinoline (HP, aka pyridinoline, Pyr) and Lysyl Pyridinoline (LP, aka deoxypyridinoline, d-Pyr), were also analyzed simultaneously as previously reported [42,43]. The cross-links were quantified as moles per mole of collagen (mol/mol of collagen).

2.5. Raman spectroscopy

The Raman system used in this study has been described previously [44]. The periosteal regions of left 7th ribs (male, n = 3 each group) were firstly analyzed at the anterior extremity (End) and mid-diaphysis (Mid). Samples were dehydrated in graded ethanol (70%, 80%, 95%, 100%), defatted in Clear-Rite 3 (Richard-Allen Scientific, Kalamazoo, MI, USA), and infiltrated in a liquid methylmethacrylate monomer (Koldmount; Mager Scientific). The bones were embedded in poly-methylmethacrylate (Koldmount Cold Mounting Kit; Mager Scientific). Using a low-speed sectioning saw (Model 650; South Bay Technology, San Clemente, CA, USA) with a diamond wafering blade (Mager Scientific), longitudinal sections (> 300 μm in thickness) were made for examining cortical bone, and were hand polished using wet silicon carbide abrasive discs [45]. At each location, End and Mid, a line-focused 785 nm laser (100 μm in length and 6–8 μm in depth) (Invictus, Kaiser Optical Systems, Inc., Ann Arbor, MI, USA) was focused on the specimen through a NIR-optimized x20 objective. Raman scatter was collected through the same objective, and delivered to a spectrograph (HoloSpec, Kaiser Optical Systems, Inc.). The Raman scatter was collected on a back-illuminated deep depletion CCD (Newton, Andor Technology, South Windsor, CT, USA). Spectral processing was performed with locally written scripts on Matlab (Math Works, Natick, MA, USA) and GRAMS/AI (Thermo Fisher Scientific, Waltham, MA, USA). Band areas were determined for select Raman peaks from bone mineral (phosphate, 959 cm^{-1}) and bone matrix (amide I, 1660 and 1690 cm^{-1}) components. For Raman metrics - the collagen cross-link ratio, i.e. Pyr to dihydroxy lysinonorleucine (DHLNL) (1660/1690) indicating cross-link maturation [46], the mineral/matrix ratio (959/[1660 + 1690]) describing the relative amount of mineralization, and crystallinity (inverse of 959 cm^{-1} bandwidth at half the peak intensity) representing mineral crystal size and perfection were calculated.

2.6. Real-time quantitative RT-PCR

RNA was isolated from the left 5th ribs (male, n = 5 each group) using Trizol reagent (Invitrogen). cDNA was synthesized using SuperScript II kit (Invitrogen). Taqman primers and probes used in this study were as follows: *Plod1*, Mm01255760_m1 (74 bp); *Plod2*, Mm00478767_m1 (77 bp); *Plod3*, Mm00478798_m1 (62 bp); *Lox*, Mm00495386_m1 (73 bp); *Loxl1*, Mm01145738_m1 (109 bp); *Loxl2*, Mm00804740_m1 (82 bp); *Loxl3*, Mm01184865_m1 (98 bp); *Loxl4*, Mm00446385_m1 (63 bp). Real-time qRT-PCR was performed (ABI 7500 PCR System; Applied Biosystems). Samples were prepared from five biological replicates and all measurements were performed in triplicate. Values were normalized to GAPDH and analyzed using the $2^{-\Delta\Delta Ct}$ method [47].

2.7. Nano-indentation

After Raman analysis, the rib sections (n = 5 each group) were used to measure the tissue-level mechanical properties by a nanoindentation system (950 TI TriboIndenter, Hysitron, Minneapolis, MN, USA) with a 0.5 μm spatial resolution. Specimens were examined visually under an optical microscope, cortical and trabecular regions of interest were located and at least five indentations each in the mid-diaphysis (Mid) and distal-metaphysis (End) were made. A diamond tip with Berkovich geometry was used to perform the indents, which consisted of a 10 μN preload, and then a 300 μN/s load rate up to 3000 μN, which was held for 10 s and then unloaded at −300 μN/s for 10 s. Five indents per compartment per sample were made with 15 μm spacing between indents. Load–displacement curves were analyzed to compute the indentation modulus (E) using the Oliver–Pharr method [48]. $1 / E_r = (1 - \nu^2) / E + (1 - \nu_i^2) / E_i$, where ν is Poisson's ratio of the indented specimen, which was set to be 0.3 assuming the bone to be an isotropic elastic material; ν_i is Poisson's ratio of the indenter tip (equal to 0.07), and E_i is the elastic modulus of the indenter material (equal to 1440 GPa). The hardness values (H) were determined by the following formula: $H = P_{max} / A$, where P_{max} is the peak indentation load and A is the projected contact area at that load. The five modulus and hardness values were averaged for each location in each sample.

2.8. Mechanical testing - four-point bending

Whole bone mechanical testing by four-point bending was performed on the left 8th ribs (males, n = 14 for controls and n = 15 for cKO) using a servo-hydraulic materials testing system (Bionix, MTS Systems Corporation, Eden Prairie, MN, USA). Whole ribs were brought to room temperature prior to testing, hydrated with calcium buffered saline solution throughout testing, and aligned in the tester with the inferior surface in tension and the vertebral end outside the right loading roller (9 mm support span, 3 mm loading span). Bones were loaded to failure at a crosshead displacement rate of 0.05 mm/s. Load and deflection data were recorded for each test and analyzed as previously described [49]. Measures of stiffness, maximum load and work-to-yield are reported.

2.9. Mechanical testing – crush test

An end mill was used to remove the end plates from the proximal and distal ends of the 4th lumbar (L4) prior to compression testing. This enabled loading of the vertebral body and provided flat surfaces of contact with the parallel compression plates. A servo-hydraulic testing machine (858 Mini Bionix II, MTS Systems, Minneapolis, MN, USA) was used and specimens were compression loaded to failure in compression at a constant displacement rate of 0.50 mm/s [50]. Ultimate load and displacement, and failure load and displacement were subsequently calculated.

2.10. Statistical analysis

All results are expressed as mean ± standard deviation (SD). Student's *t*-tests were used to compare data between control and cKO mice in each gender; $p < 0.05$ indicates significance.

3. Results

3.1. Osteoblast-specific disruption of Bmpr1a results in more bone mass in rib cortical compartments

In this study, we investigated the role of BMPR1A on bone mass, composition and biomechanical properties in flat bones using rib bones from mice at 22-week. We previously reported higher bone mass in cKO ribs by histologic observation, including larger cortical thickness and

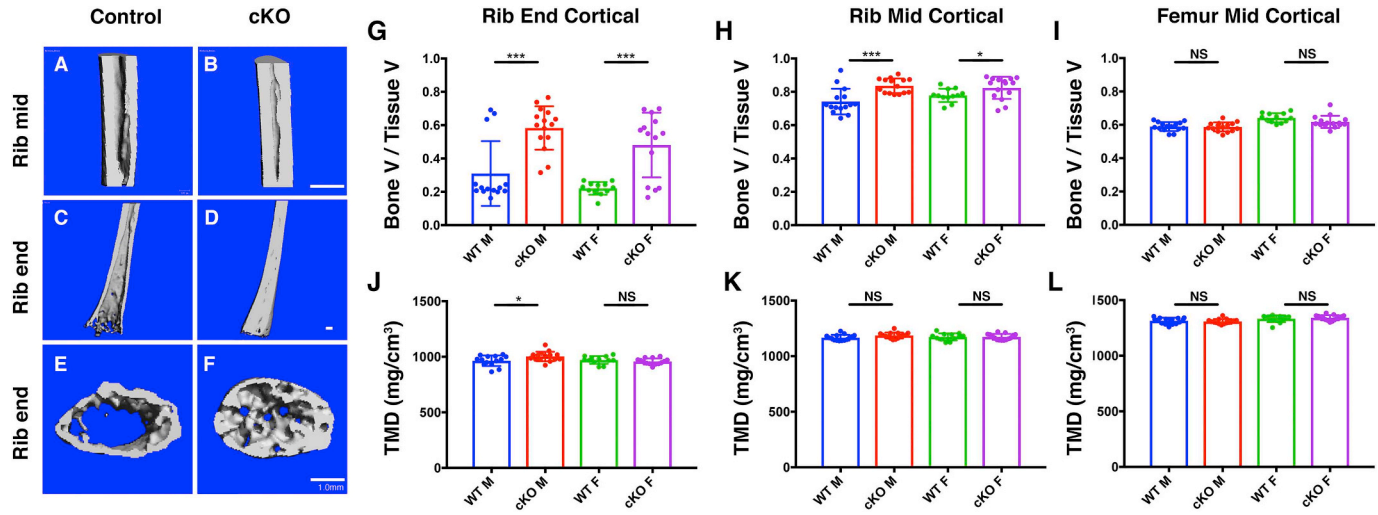

Fig. 1. Loss of BMPR1A resulted in increased cortical bone mass in rib bones. Representative 3D reconstitution μCT images of the 6th rib from a 22-week old male. Mid and End portion of sagittal views for cortical compartments and End portion of transverse views for trabecular compartments are shown. Parameters from End and Mid rib cortical compartments are shown at center left and center right, respectively. μCT measurements of femur from the same mice are also shown for comparison (right). Blue bars, control male mice (WT M, n = 14 for rib End, n = 15 for rib Mid, n = 14 for femur), red bars, cKO male mice (cKO M, n = 15 for rib End, n = 15 for rib Mid, n = 15 for femur), green bars, control female mice (WT F, n = 12 for rib End, n = 12 for rib Mid, n = 15 for femur), purple bars, cKO female mice (cKO F, n = 14 for rib End, n = 15 for rib Mid, n = 15 for femur). Mean ± SD, *t*-test; *, $p < 0.05$, ***, $p < 0.001$, NS, not significant. (For interpretation of the references to colour in this figure legend, the reader is referred to the web version of this article.)

trabecular volumes at 34-week [21,22]. Similarly, at 22-weeks, μCT analyses showed significantly greater bone mass in cKO ribs, both in the metaphysis region (End) and the mid-diaphysis region (Mid) (Fig. 1A–F). The bone volume per tissue volume (BV/TV) was significantly greater in the cortical compartments of the male and female cKO ribs at the End regions (Fig. 1G). BV/TV was significantly higher in the cortical compartments at the Mid regions (Fig. 1H). These changes were in contrast with the mid region of femur cortical compartments from the same mice examined in the study where the cKO femur showed no significant changes in both genders (Fig. 1I). Except male End samples, there was no significant changes in cortical TMD (Fig. 1J, K), which is similar to that in femoral cortical bones (Fig. 1L). These results suggest that loss of BMPR1A signaling in osteoblasts increases cortical bone mass of ribs differently compared to the femur.

For the trabecular compartments, we focused on the End part because the amount of trabecular bones in the mid region of the control ribs was negligible. Both cKO males and females showed significantly greater BV/TV and BMD (Figs. 1E, F and 2A, E) contrasting the data from the femur (Fig. 2B, F). No differences in TMD were found in cKO ribs, but higher TMD was found in cKO femur in both genders (Fig. 2I, J). Both cKO ribs and femur showed slight but significantly lower trabecular numbers in males and significantly greater trabecular thickness in both genders (Fig. 2C, D, G, H). Since both genders showed similar changes in bone parameters, we focused on male mice for biochemical, spectroscopic, molecular and biomechanical analyses.

3.2. Osteoblast-specific disruption of *Bmpr1a* results in higher levels of mature collagen cross-links in ribs

To explore the effect of BMPR1A on collagen content and cross-link in ribs, we first measured collagen composition and collagen content by % of collagen in total protein and μg of collagen/mg dry weight, respectively. In both 10-week and 22-week samples, there were no significant differences in collagen composition between control (62.3 ± 16.4% at 10-week and 54.4 ± 6.7% at 22-week samples) and cKO (56.9 ± 21.3% and 47.9 ± 13.7%) (Fig. 3A) or in collagen content between control (172.2 ± 8.3 μg/mg and 175.0 ± 9.3 μg/mg) and cKO (161.8 ± 25.0 μg/mg and 167.3 ± 21.2 μg/mg) (Fig. 3C). Moreover, the Hyl content in collagen did not show a significant difference between control (42.5 ± 9.2 mol/mol collagen and 36.0 ± 13.9 mol/mol collagen) and cKO (43.3 ± 7.1 mol/mol collagen and 36.0 ± 13.9 mol/mol collagen) (Fig. 3B). These results suggested that BMP signaling through BMPR1A in osteoblasts does not play a significant role in the amount of collagen and its overall Lys hydroxylation in the rib.

Next, we characterized collagen cross-links. The contents of the two non-reducible cross-links (HP and LP) were depicted in Fig. 2D–F. There are significant increases in HP (*$p < 0.05$ at 10-week and **$p < 0.01$ at 22-week old, Fig. 3D), LP (*$p < 0.05$ at 22-week old, Fig. 3E) and HP + LP (*$p < 0.05$ at 10-week and **$p < 0.01$ at 22-week old, Fig. 3F) between control and cKO. These results suggest that loss of BMPR1A increases the levels of the mature, stable collagen cross-links.

3.3. Loss of BMPR1A signaling increased cross-link collagen mature to immature ratios and mineral to matrix ratios in ribs

By employing Raman spectroscopy, bone composition in local areas of rib bones was analyzed, with focus on cortical compartments of the End and Mid regions of each bone. For collagen cross-links, the relative % area of the individual underlying bands (1660 and 1690 cm^{-1}, representative of HP (mature) and DHLNL (immature) collagen cross-links, respectively) were plotted. Increased ratios of mature to immature in the Mid of cortical were identified (Fig. 4A). Since collagen fibrils serve as a template of mineralization, the status of collagen cross-links found in the *Bmpr1a* cKO bones may affect the mineralization process. We therefore examined the relative amounts of mineral and matrix (mineral-matrix ratio, MMR) and crystallinity of ribs. There were no significant differences in MMR and crystallinity in either the End or Mid portions of rib cortical compartments between control and cKO (Fig. 4B, C). These data along with biochemical analyses suggest that disruption of *Bmpr1a* in osteoblasts increases mature cross-links in ribs, but has less impacts on the amounts, or size of the mineral.

3.4. Disruption of BMPR1A signaling upregulates collagen post-translational modifying genes

Enzymatic cross-link formation has been found to have a positive effect on mechanical strength of bone within a beneficial level [51].

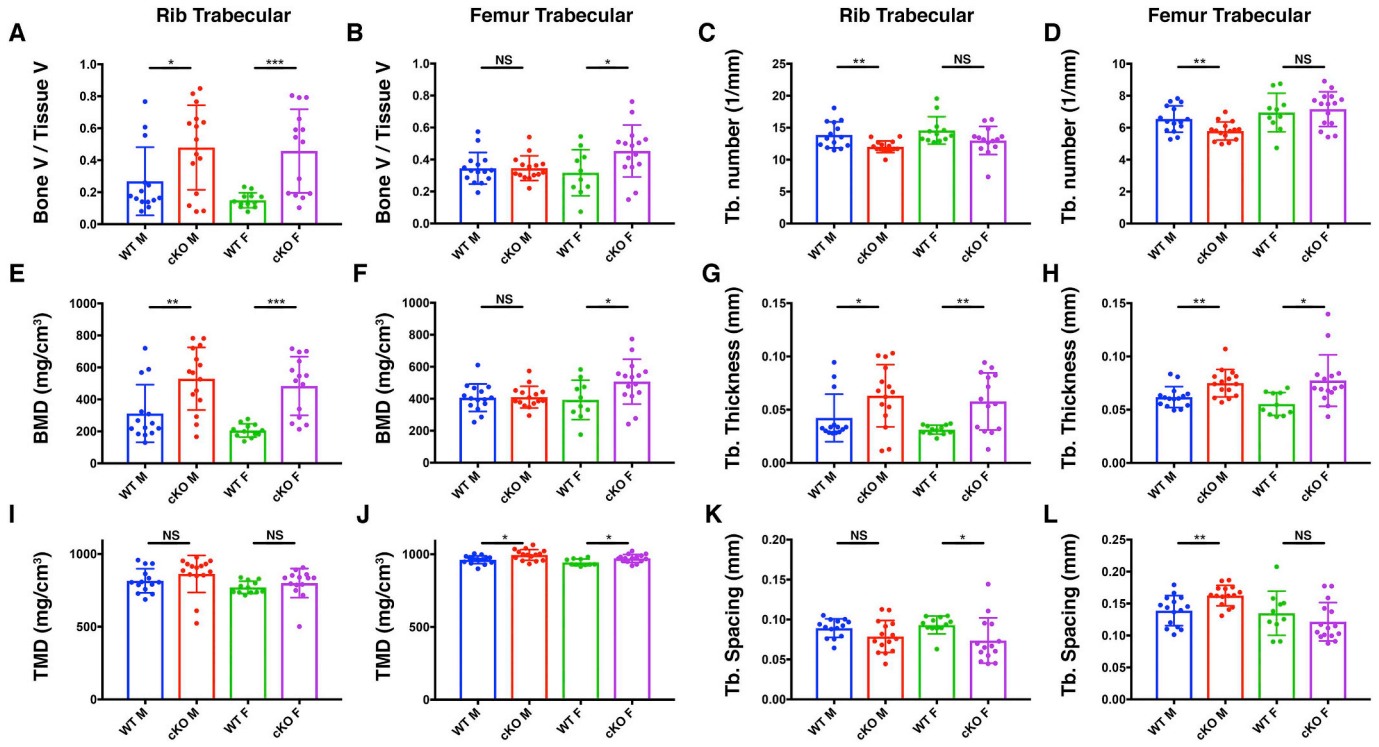

Fig. 2. Loss of BMPR1A resulted in increased trabecular bone mass in rib bones. Six parameters for trabecular measurements of the 6th rib from 22-week old males and females are shown (left and center right). μCT measurements of femur from the same mice are also shown for comparison (center left and right). Blue bars, control male mice (WT M, n = 14 for rib, n = 15 for femur), red bars, cKO male mice (cKO M, n = 15 for both bones), green bars, control female mice (WT F, n = 12 for rib, n = 10 for femur), purple bars, cKO female mice (cKO F, n = 15 for both bones). Mean ± SD, *t*-test; *, $p < 0.05$, **, $p < 0.01$, ***, $p < 0.01$, NS, not significant. (For interpretation of the references to colour in this figure legend, the reader is referred to the web version of this article.)

The critical enzymes that regulate collagen cross-linking include: lysyl hydroxylase 1–3 (LHs), lysyl oxidase, and lysyl oxidase like 1–4 (LOXs) respectively [52]. To explore the potential effect of BMPR1A signaling on the gene expression of these modifying enzymes, we examined expression of *Plod1*, *2*, and *3* (encoding LH1, 2, 3), *Lox*, *Loxl1*, *2*, *3* and *4* in ribs. QRT-PCR results showed only *Loxl4* was significantly up-regulated in the cKO comparing with controls (*$p < 0.05$, Fig. 5) while others did not reach the significant levels (Fig. 5). These results suggest a possibility that absence of BMPR1A signaling may increase only specific gene expression related to collagen cross-linking, which may lead to an alteration of collagen cross-links with higher levels of HP and LP.

3.5. Disruption of BMPR1A improved whole bone strength in ribs

To determine whether the loss of BMPR1A signaling influenced biomechanical properties in ribs, we measured intrinsic properties (tissue-level biomechanical properties) by nanoindentation tests on rib cortical and trabecular compartments. In the both cortical and trabecular compartments, there were no significant differences in hardness and elastic modulus between cKO and control samples (Fig. 6A–D).

Bone contains two phases, collagen and mineral, and both phases contribute to toughness (capacity to absorb energy) and bone stiffness. To understand how these changes in collagen and mineral resulting from BMPR1A deficiency affect other bone biomechanical properties, we performed four point bending of rib diaphyses for both genders. The results of this whole bone level analysis revealed a significant increase in stiffness in females and maximum load in both males and females in the cKO mice (*$p < 0.05$, **$p < 0.01$, Fig. 7A, B). BMPR1A deficiency resulted in a significant increase in work to yield only in male ribs (**$p < 0.01$, Fig. 7C). These results indicate loss of BMPR1A was associated with greater resistance to the external loading at the whole bone level.

3.6. Osteoblast-specific disruption of Bmpr1a increased bone mass and bone strength in lumbar vertebra

The rib cortex responded to the loss of BMPR1A in an opposite manner to the femoral cortex in terms of bone mass and mechanical properties. Since BMP signaling through BMPR1A may play different roles in the axial skeleton like ribs and the appendicular skeleton like femora, we choose another axial bone of the lumbar spine and investigated the bone mass and biomechanical properties. Bone mass of the 4th lumbar vertebrae (L4) was examined by μCT. The cortical compartments showed a significantly higher degree of TMD, increased cortical thickness and cross-sectional area in the cKO for males and females (Table 1). In trabecular compartments, a significantly higher degree of TMD, increased bone volume fraction and trabecular thickness were observed in the cKO for males and females (Table 2). These results suggested loss of BMPR1A in osteoblasts increased bone mass both in cortical and trabecular bone of the lumbar vertebra. The data from cortical bones indicated BMPR1A deficiency increased bone mass in both ribs and lumbar cortical bones. These observations are different from the data from femora, which showed minimal impacts on bone mass with loss of BMPR1A (Fig. 1I, L).

To understand whether the increased lumbar mass by BMPR1A disruption can contribute to greater bone strength, the L4 were assessed by a compression test. The results showed larger ultimate load and failure load by 79% and 78% compared with controls in the cKO males (*$p < 0.05$, Table 3), while those were not affected in bones from females. There were no significant differences between control and cKO bones in ultimate displacement and failure displacement (Table 3). The difference of genders can be explained by μCT parameters. Tissue mineral density of cortical and trabecular bones were increased significantly in males compared with females. Male cKO bones showed 16% higher in cortical tissue mineral density (**$p < 0.01$, Table 1) and 25% higher in trabecular mineral density (**$p < 0.01$, Table 2).

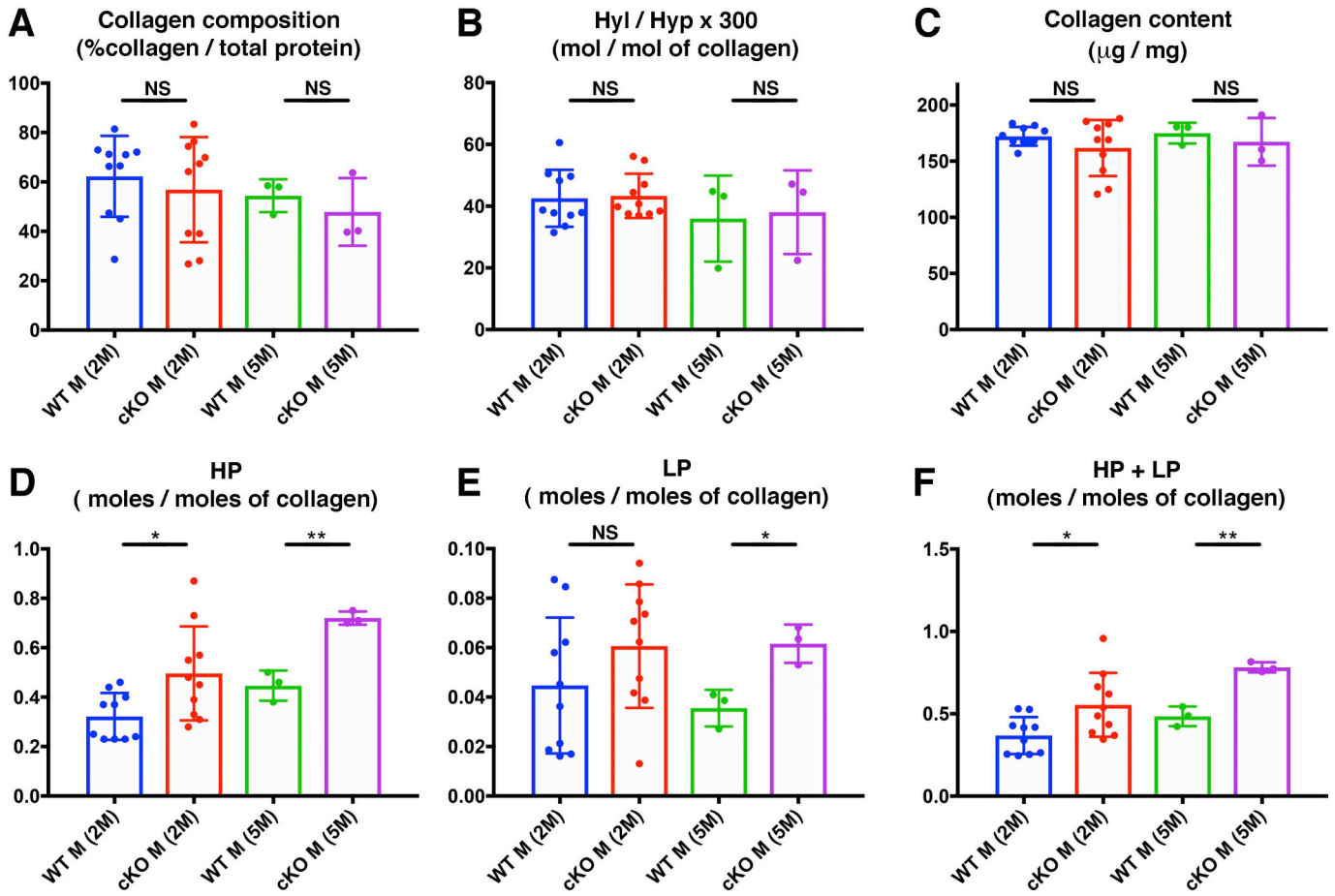

Fig. 3. Loss of BMPR1A resulted in more non-reduced mature cross-links of collagen in ribs. Collagens were extracted from 6th ribs of 10-week (2 M) or 22-week (5 M) males and subjected biochemical analyses followed by HPLC separation to quantify mature cross-links. There were no statistical differences between control and cKO in collagen composition (A, % collagen/total protein), the ratio of Hyl/Hyp (B, the extent of Lys hydroxylation of collagen) and collagen contents (C, Hyp/dry ash), whereas the mature cross-links HP (D), LP (E) and HP + LP (F) were higher in cKO ribs than in controls. Blue and green bars, control male mice (WT M), red and purple bars, cKO male mice (cKO M), n = 5 for 10-week (2 M) group and samples from left and right sides were analyzed separately (blue and red bars). n = 3 for 22-week (5 M) group and samples from left and right sides from the same animal were combined and analyzed (green and purple bars). Mean ± SD, *t*-test; *, $p < 0.05$, **, $p < 0.01$, NS, not significant. Hyl, hydroxylysine; Hyp, Hydroxyproline; HP, hydroxylysylpyridinoline; LP, lysylpyridinoline. (For interpretation of the references to colour in this figure legend, the reader is referred to the web version of this article.)

Comparing with males, female cKO bones showed 4% (**$p < 0.01$, Table 1) and 19% (**$p < 0.01$, Table 2) higher in those parameters. These results suggested loss of BMPR1A increase whole bone strength of lumbar vertebra due to elevated bone mass in a gender-biased manner in lumbar vertebra.

4. Discussion

In this study, we have demonstrated that loss of BMP signaling in osteoblasts mediated by BMPR1A results in overlapped and unique outcomes in ribs, vertebrae and femur. We previously reported that the cortical compartments of the cKO femora and tibiae show reduced cortical surface area with increased cortical porosity but unchanged bone compositions such as collagen and mineral contents along with unchanged tissue-level biomechanical properties. The decreased cortical area and increased porosity without compensation of tissue-level mechanics are associated with reduced whole bone levels of biomechanical properties [30,31]. In contrast, in the present study, the cKO ribs showed increased bone mass in the cortical compartments with small changes in collagen cross-links but no overt changes in mineral to matrix ratio (MMR) and crystallinity. The increase in bone mass in the cKO ribs without alterations in compositions were associated with an increased whole bone level biomechanical properties. Similar to the ribs, increased bone mass is found in the cortical compartments of the cKO spine with increased tissue mineral density. It is suggested that those alterations together result in increased whole bone level biomechanical properties.

In the trabecular compartments of the cKO femora and tibiae, we have reported that bone mass is increased in association with a higher ratio of mature to immature collagen cross-links, a higher mineral to matrix ratio (MMR) and a higher tissue mineral density with improved tissue-level biomechanical properties [30,53]. The cKO ribs and cKO spines showed similar changes in terms of bone mass, but tissue mineral density in cKO ribs did not change while that in cKO spines showed an increase. Unlike the trabecular compartments of cKO femora, that of cKO ribs did not show alterations in tissue-level biomechanical properties. It is still possible to contribute to increased whole bone level biomechanical properties due to highly increased trabecular bone mass in the midshaft of the cKO ribs.

4.1. Increased bone mass in the cortical compartment is the likely major parameter for improved biomechanical properties

Our analysis demonstrated increased bone mass in the trabecular compartments of ribs and lumbar spines (Fig. 2 and Table 2), which is consistent with observations in long bones from us [21–23,31,53] and others [25,26]. Given the previous studies, loss of *Bmpr1a* in osteoblasts leads to decreased osteogenesis and secondarily decreased

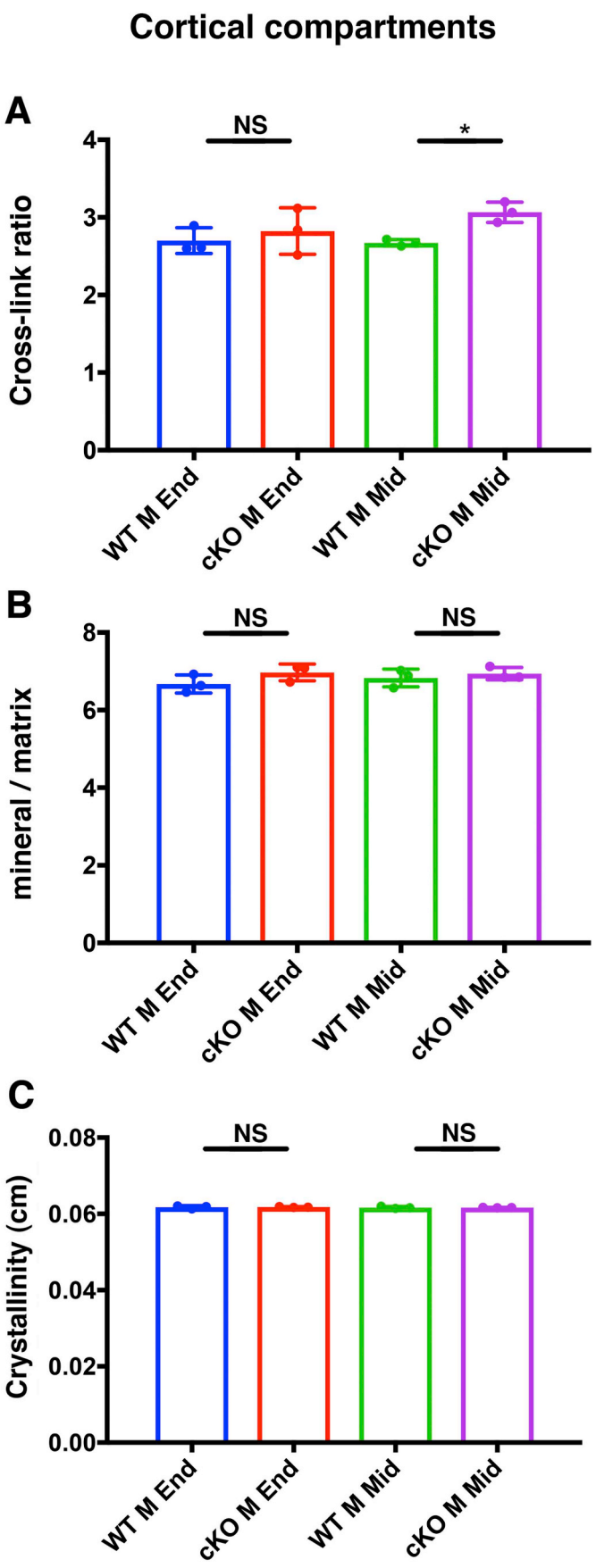

Fig. 4. Loss of BMPR1A resulted in more mature to immature collagen cross-links in rib midshafts. The ratio of collagen mature/immature, mineral to matrix ratio and crystallinity were measured using 7th rib of at 22-week males. The regions were focus on the anterior extremity (End) and mid-diaphysis (Mid) of cortical compartments. BMPR1A cKO ribs showed larger ratios in mature collagen cross-links in the cortical compartments of Mid (A) regions. There were no significant differences in the mineral to matrix ratios (B) and crystallinity between two genotypes (C). Blue bars, control male mice (WT M), red bars, cKO male mice (cKO M), green bars, control female mice (WT F), purple bars, cKO female mice (cKO F). Mean ± SD, t-test; *, $p < 0.05$, NS, not significant; $n = 3$ each. (For interpretation of the references to colour in this figure legend, the reader is referred to the web version of this article.)

osteoclastogenesis. The more negatively affected bone resorption lead to increased bone mass, which is one of the factors that contribute to the increased bone mass.

We also demonstrated increased bone mass in the cortical compartments of ribs and lumbar spines (Fig. 1 and Table 1), which is a contrasting outcome from changes we have reported in long bones [30,31]. *Bmrp1a* cKO long bones show reduced whole bone levels of biomechanical properties [30,31] whereas *Bmrp1a* cKO ribs and spine show improved whole bone levels of biomechanical properties (this study) likely due to the increased bone mass, but not the alterations in composition as discussed below.

Collagen cross-linking is an important factor to influence bone strength [54]. In most cases, increased levels of mature collagen cross-links are advantageous for bone strength. Here, we found increased levels of HP and LP, both are mature, stable cross-links, in the mutant ribs assessed by biochemical analysis (Fig. 3) and an increased mature to immature cross-link ratio in the mutant cortical compartments by Raman spectroscopic analysis (Fig. 4). The expression of genes that encode collagen cross-link associated enzymes, except *Loxl4*, were not significantly changed in the mutant ribs (Fig. 5). It is possible that upregulation of *Loxl4* in the cKO ribs may lead to increased cross-links in collagens. As of today, potential involvement of LOXL4 to increase osteoblast functions have been suggested [55,56] but no report is available to describe its involvement in vivo bone homeostasis. However, considering the facts that all other gene expression as well as Lys hydroxylation levels did not show differences and an increased ratio of mature (HP) to immature (DHLNL) cross-links, the increases in mature cross-links may result from a slower collagen turnover since both bone forming and bone resorbing activities are lowered in the *Bmpr1a* cKO bones [22,23,30]. This notion is also supported by previous studies. For instance, similar changes in cross-linking profile, i.e. increased mature cross-links and an increased ratio of mature to immature cross-links is reported, in osteopetrotic bones in which bone remodeling is severely suppressed [57]. By comparing matrix compositions between flat and long bones, van den Bos et al. and Matsuura et al. also reported that higher levels of HP (mature) cross-link in the latter may cause slower bone resorption [58,59]. A more extensive cross-link analysis including precursor aldehydes, immature and mature cross-links in *Bmpr1a* cKO bones is warranted to obtain further insight into this possibility. Since we used dehydrated samples for nanoindentation tests (Fig. 6), we were not able to collect parameters for collagen modifications. We did not detect significant differences in tissue-level properties between two genotypes (Fig. 6) suggesting that increased whole bone level biomechanical properties in the mutant ribs (Fig. 7) may be driven by an increase of bone mass rather than alterations in composition of bones.

4.2. Why did different bones show different phenotypes in Bmpr1a cKO mice?

Our study highlights that bones in different anatomical regions and formed through different developmental processes respond differently to loss of BMP signaling mediated by BMPR1A in the osteoblast lineage. While bone mass of the trabecular compartments in long bones, ribs and

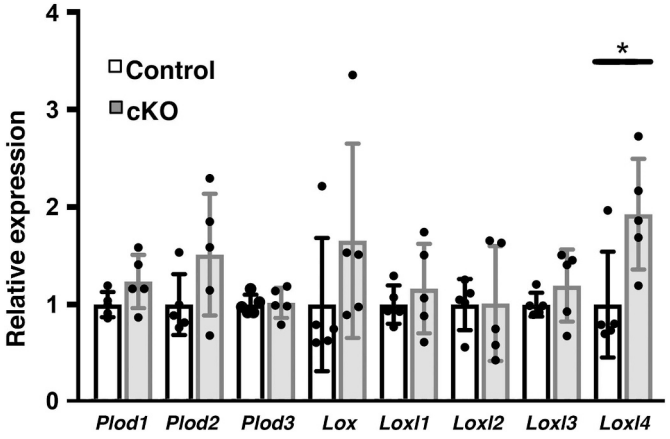

Fig. 5. Collagen post-translational modification related genes were increased in *Bmpr1a* cKO bones. RNA was extracted from rib 7th at 22 week (male) and levels of gene expressions were measured by QRT-PCR. Expression levels of *Plod4* were significantly greater in the cKO. *Plod1* showed tendency to increases. RNA from 5 bones were used to set up triplicate reactions for each bone. Open bars, control male mice, grey bars, cKO male mice. Mean ± SD, *t*-test; *, $p < 0.05$; $n = 5$ each.

spines are increased in cKO mice, mineral density is increased in long bones and spines, but not in ribs (Fig. 2 and Table 2). Bone mass in the cortical compartment of cKO spines is increased with an increase of mineral density, while cKO ribs showed increased bone mass without overt changes in mineral density (Fig. 1 and Table 1). One possible explanation for these different outcomes is differences in expression levels of each BMP receptor in different anatomical locations. Osteoblast-specific disruption of another BMP type 1 receptor *Acvr1* results in nearly identical phenotypes in long bones [27] suggesting that in bones where *Acvr1* expression is higher than other bones, an impact of the loss of *Bmpr1a* may be less robust. Quantification of expression levels of each receptor and signaling component in different bones should shed a light in this direction.

There are a limited number of reports to compare how different bones respond differently to other factors such as ages and genetic mutations. Results from The Osteoporotic Fractures in Men (MrOS), a multicenter prospective cohort study, reveal that area BMD of the femoral neck and lumbar spine are associated with an increased risk of fracture at the hip, spine, rib and other non-spine fracture [60]. The same study shows an association between lower trabecular femoral neck and spine volumetric BMD and increased risks of most fractures while femoral neck volumetric BMD itself is associated with only fracture risk of the hip and spine sites [60]. Ovariectomized sheep lose bone mass to a different degree in different bones, i.e. in lumbar BV/TV is decreased by 45.6% while only by 18.7% in rib [61]. Teriparatide has been used to improve bone mass in osteoporotic patients. Interestingly, 52 patients ranging from 43 to 87 years old treated by teriparatide show increased BMD by DEXA and CT in the lumbar spine without change in femoral BMD [62]. The Viva La Familia Study is a family-based cohort with a total of 1030 Hispanic children ranging from 4 to 19 years old. This study identifies linkages for BMD of pelvis and left leg on chromosome 7p14, lumbar spine on 20q13 and left rib on 6p21, and BMC of pelvis on chromosome 20q12 and total body on 14q22-23 [63]. Genome-wide association studies using the same cohort reveal that associations between BMC of right arm and rs762920 at PVALB and between pelvis BMD and rs7000615 at PTK2B [63]. Those data strongly suggest that homeostasis of different bone may be fine-tuned by different sets of genetic components.

Bones in different anatomical locations may require different functions to accommodate different mechanical environment during bone development and postnatal life. Long bones are distributed on the

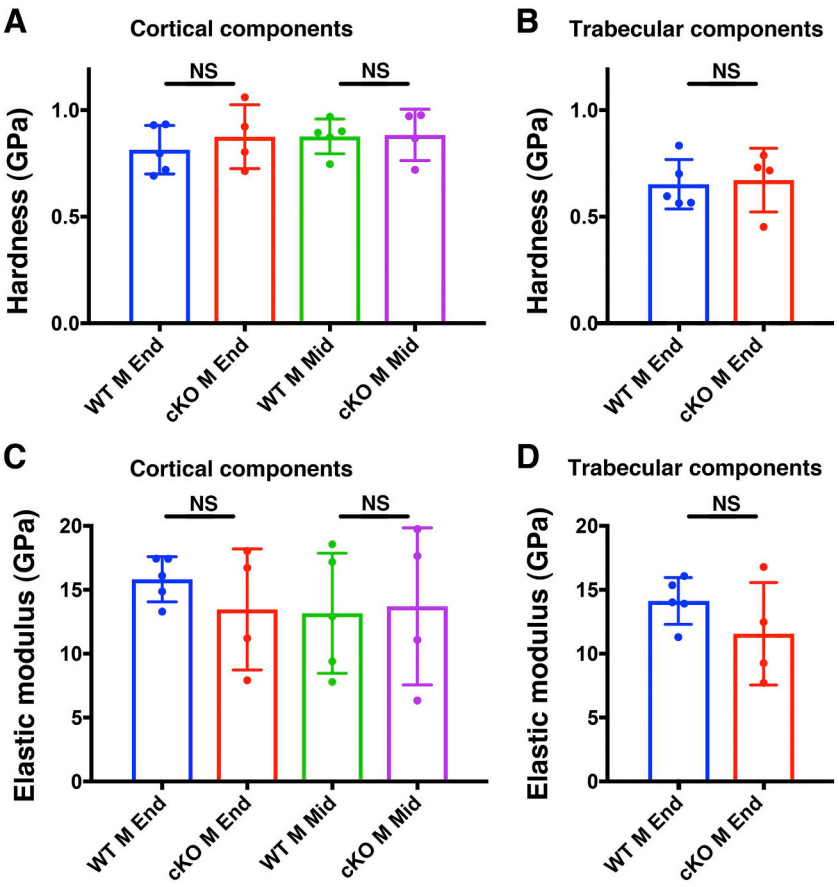

Fig. 6. Nanoindentation measurements of tissue-level biomechanical properties in the distal metaphysis (End) and mid-diaphysis (Mid) of the cortical compartment (A, C) and End region of the trabecular compartment (B, D) of the rib from 22-week male mice. None of the measurements showed significant differences. Blue bars, control male mice at End (WT M End), red bars, cKO male mice at End (cKO M End), green bars, control male mice ad Mid (WT M Mid), purple bars, cKO male mice at Mid (cKO M Mid). Mean ± SD, t-test; NS, not significant; $n = 5$ for control End cortical, control End trabecular and cKO Mid cortical compartments. $n = 4$ for control Mid cortical, cKO End cortical, and cKO End trabecular compartments. (For interpretation of the references to colour in this figure legend, the reader is referred to the web version of this article.)

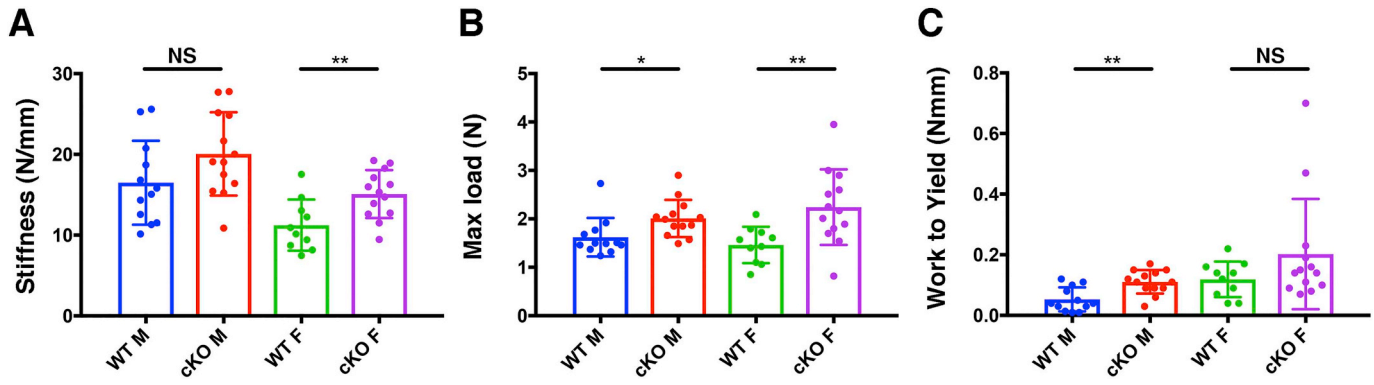

Fig. 7. The effect of loss of BMPR1A on biomechanical properties in rib was assessed by 4-point bending tests. The mid-diaphysis of 8th rib was analyzed in males and females after microCT. The max load (B) was significantly increased in the cKO in both genders compared with the control, whereas stiffness (A) was increased only in the female cKO mice and work to yield (C) was increased only in the male cKO mice. Blue bars, control male mice (WT M, n = 12), red bars, cKO male mice (cKO M, n = 13), green bars, control female mice (WT F, n = 10), purple bars, cKO female mice (cKO F, n = 13). Mean ± SD, *t*-test; *, $p < 0.05$; **, $p < 0.01$; NS, not significant. (For interpretation of the references to colour in this figure legend, the reader is referred to the web version of this article.)

Table 1
microCT analyses of the 4th lumbar vertebrae (L4), cortical compartments, 34 week old mice.

	Lumbar 4 (male)		Lumbar 4 (female)	
Parameters (unit)	Control (n = 10)	cKO (n = 10)	control (n = 10)	cKO (n = 10)
Cortical thickness (mm)	0.220 ± 0.02	0.473 ± 0.11**	0.197 ± 0.02	0.382 ± 0.08**
Cross sectional area (mm^2)	1.175 ± 0.21	1.985 ± 0.49**	1.211 ± 0.16	1.619 ± 0.33**
Tissue mineral density (mg/cm^3HA)	809.306 ± 27.34	937.459 ± 47.15**	875.254 ± 12.61	913.745 ± 21.74**

Loss of BMPR1A resulted in greater cortical bone mass in spines.
Mean ± SD, *t*-test.
** $p < 0.01$.

Table 2
microCT analyses of the 4th lumbar vertebrae (L4), trabecular compartments, 34 week old mice.

	Lumbar 4 (male)		Lumbar 4 (female)	
Parameters (unit)	Control (n = 10)	cKO (n = 10)	Control (n = 10)	cKO (n = 10)
BV/TV (mm^3/mm^3)	0.601 ± 0.08	0.831 ± 0.14**	0.401 ± 0.09	0.725 ± 0.15**
Trabecular number (1/mm)	6.32 ± 0.75	4.32 ± 1.73**	5.34 ± 1.09	4.60 ± 1.41**
Trabecular thickness (mm)	0.099 ± 0.02	0.262 ± 0.17**	0.071 ± 0.02	0.195 ± 0.13**
Trabecular spacing (mm)	0.063 ± 0.01	0.037 ± 0.02**	0.127 ± 0.02	0.056 ± 0.02*
Tissue mineral density (mg/cm^3HA)	568.382 ± 49.38	711.192 ± 87.56**	539.505 ± 35.88	706.447 ± 57.45**

Loss of BMPR1A resulted in greater trabecular bone mass in spines.
Mean ± SD, *t*-test.
* $p < 0.05$.
** $p < 0.01$.

Table 3
Compression testing of the 4th lumbar vertebrae (L4), 34 week old mice.

	Lumbar 4 (male)		Lumbar 4 (female)	
Parameters (unit)	Control (n = 10)	cKO (n = 10)	Control (n = 10)	cKO (n = 10)
Ultimate load (N)	30.72 ± 14.56	55.08 ± 20.50*	37.96 ± 21.86	49.55 ± 30.28
Failure load (N)	30.70 ± 14.56	55.02 ± 20.52*	37.94 ± 21.86	49.48 ± 30.26
Ultimate displacement (mm)	0.200 ± 0.10	0.262 ± 0.17	0.182 ± 0.10	0.212 ± 0.13
Failure displacement (mm)	0.203 ± 0.01	0.231 ± 0.12	0.184 ± 0.10	0.215 ± 0.13

The mechanical properties of ultimate load (A) and failure load (B) were significantly larger in the cKO male. Ultimate displacement (C) and failure displacement (D) were not significantly different between controls and cKOs in either gender.
Mean ± SD, *t*-test.
* $p < 0.05$.

extremities to bear loads. The flat bones have microscopic shape to disperse stress and form walls of body cavities such as the cranial cavity and the thorax cavity to protect important organs in the cavity. The mechanical environment is an essential factor in skeletal development and fracture repair [64–66]. Thus, it is possible to speculate that different mechanical environment may influence characters of bone cells

in each bone to behave differently in response to, for example, loss of BMP signaling.

Differences in developmental origins of each bone may be another potential reason to explain their different behavior. Ribs and spines are developed from the paraxial mesoderm whereas long bones formed in the limbs are from the lateral plate mesoderm. Studies using quail-chick chimaeras followed by lineage tracing studies in mice establish an idea that the frontal bone in the skull arises from neural crest lineage, while the parietal bone is of mesodermal lineage [67,68]. Mesenchymal stem cells from the frontal bone are more proliferative and osteogenic, and are impacted to a greater degree by normal and aberrant FGF signaling and other factors [69,70]. There is almost no information available regarding how bone cells in ribs and spines behave differently from those in long bones. It is reported that loss of beta-catenin in *Col1*-expressing cells affect different bones differently, i.e. resulting in highly aggressive osteoclastogenesis in the rib leading to fracture while impacts on femora and spine are modest [33]. This is likely due to an unusually high expression of RANKL in osteoblasts in the rib [33]. The limb mesenchyme-specific disruption of *Sost* results in modest increase of trabecular BV/TV in the vertebrae where cells should express normal levels of *Sost* [71]. One possible explanation is that cells in the vertebrae would be more sensitive for availability of SOST/Sclerostin than cells in the femora, since SOST protein in serum is reduced in half in the cKO mice [71]. In the bone from *Col1*-expressing cell-specific disruption of *Bmpr1a*, we have shown that Wnt-canonical pathway is highly upregulated due to the highly significant reduction of *Sost* expression in osteoblasts [21–23]. We also demonstrated that a reduction of *Rankl* expression accompanied with greater expression of *Opg* in *Bmpr1a* mutant osteoblasts [22,23]. Indeed, mutant osteoblasts from the *Bmpr1a* cKO femora fail to support osteoclastogenesis in culture [23]. Taken together, one potential explanation of anatomical location dependent outcome of the impact of loss of BMP signaling may be that osteoblasts in different bones differentially regulate osteoclastogenesis upon loss of BMP signaling. Future studies are awaiting to elucidate side-by-side characterization of osteoblasts from different bones for their bone forming activities and supporting activities for osteoclastogenesis.

5. Conclusion

In this study, we have shown that loss of BMP signaling mediated by BMPR1A in the osteoblast lineage results in increased bone mass in both cortical and trabecular compartments of ribs and spines while minimal to modest compositional changes were observed. Some of those changes were different from what we have reported in long bones. These data suggest that the function of BMP signaling in osteoblasts through BMPR1A may be specific depending on anatomical location, possibly due to their developmental origins. Suppression of BMPR1A mediated BMP signaling by administration of a soluble form of BMPR1A to wild type mice prevents ovariectomy-induced bone loss and improves bone strength [29]. Thus, it is an interesting future endeavor to suppress BMP signaling aiming to increase bone mass to reduce fracture risk.

Author contributions

HZ, YZ, NK and YM contributed to conception, design, and data analysis, drafted the manuscript. HZ, YZ, YL, MO and NK contributed to histological and molecular analyses. YZ, YL, DMJ, EIW, ML, RZ, DHK and YM contributed to micro-CT analysis. MT and MY contributed to collagen analyses. PZ, MR and MDM contributed to Raman spectrometry. GR, EB, DMJ, EIW, NK, KJJ, SG ad DHK contributed to biomechanical analyses. YZ, NK and YM provided critical materials. All approved the final version of the manuscript. HZ, YZ and YM take responsibility for the integrity of the data analysis.

CRediT authorship contribution statement

Honghao Zhang: Conceptualization, Methodology, Validation, Data curation, Writing - original draft, Writing - review & editing. **Yanshuai Zhang:** Conceptualization, Methodology, Validation, Data curation, Writing - original draft. **Masahiko Terajima:** Methodology, Validation, Data curation, Writing - original draft. **Genevieve Romanowicz:** Methodology, Validation, Data curation. **Yangjia Liu:** Methodology, Validation, Data curation, Writing - original draft. **Maiko Omi:** Methodology, Validation, Data curation. **Erin Bigelow:** Methodology, Validation, Data curation. **Danese M. Joiner:** Methodology, Validation, Data curation, Writing - original draft. **Erik I. Waldorff:** Methodology, Validation, Data curation, Writing - original draft. **Peizhi Zhu:** Methodology, Validation, Data curation. **Mekhala Raghavan:** Methodology, Validation, Data curation, Writing - original draft. **Michelle Lynch:** Methodology, Validation, Data curation. **Nobuhiro Kamiya:** Conceptualization, Methodology, Validation, Data curation, Writing - original draft, Writing - review & editing. **Rongqing Zhang:** Methodology, Supervision. **Karl J. Jepsen:** Conceptualization, Methodology, Validation, Writing - review & editing, Supervision. **Steve Goldstein:** Conceptualization, Methodology, Validation, Writing - review & editing, Supervision. **Michael D. Morris:** Conceptualization, Methodology, Validation, Writing - review & editing, Supervision. **Mitsuo Yamauchi:** Conceptualization, Methodology, Validation, Writing - review & editing, Supervision. **David H. Kohn:** Conceptualization, Methodology, Validation, Writing - review & editing, Supervision. **Yuji Mishina:** Conceptualization, Methodology, Validation, Writing - original draft, Writing - review & editing, Supervision, Project administration, Funding acquisition.

Acknowledgments

The authors thank Drs. Tatsuya Kobayashi and Hank Kronenberg for Col1-CreER mice and Greg Stott and Manas Ray for initial contribution of sample preparations. We also thank Drs. Gurjit Mandair for advice on Raman analyses, Kenneth Kozloff and Joseph Perosky for advice on nanoindentation, and Taocong Jin for help in qRT-PCR analysis. This study is supported by the National Institutes of Health; United States NIDCR R01DE020843 to YM, R03DE027456 to HZ and F30DE028167 to GR, and by a core grant from the NIAMS P30 AR069620 to Karl Jepsen, PI; David H. Kohn, Core Director. The micro-CT core at the University of Michigan School of Dentistry is funded in part by NIH/NCRR S10RR026475-01. The content is solely the responsibility of the authors and does not necessarily represent the official views of the NIH.

References

[1] N. Kamiya, Y. Mishina, New insights on the roles of BMP signaling in bone-a review of recent mouse genetic studies, Biofactors 37 (2011) 75–82.
[2] M. Urist, Bone: formation by autoinduction, Science (1965) 893–899.
[3] I. Grafe, S. Alexander, J.R. Peterson, T.N. Snider, B. Levi, B. Lee, Y. Mishina, TGF-beta family signaling in Mesenchymal differentiation, Cold Spring Harb. Perspect. Biol. 10 (2018).
[4] J.W. Lowery, V. Rosen, The BMP pathway and its inhibitors in the skeleton, Physiol. Rev. 98 (2018) 2431–2452.
[5] S. Lin, K.K. Svoboda, J.Q. Feng, X. Jiang, The biological function of type I receptors of bone morphogenetic protein in bone, Bone Res. 4 (2016) 16005.
[6] J.L. Wrana, L. Attisano, R. Wieser, F. Ventura, J. Massague, Mechanism of activation of the TGF-beta receptor, Nature 370 (1994) 341–347.
[7] Y. Chen, A. Bhushan, W. Vale, Smad8 mediates the signaling of the ALK-2 [corrected] receptor serine kinase, Proc. Natl. Acad. Sci. U. S. A. 94 (1997) 12938–12943.
[8] P.A. Hoodless, T. Haerry, S. Abdollah, M. Stapleton, M.B. O'Connor, L. Attisano, J.L. Wrana, MADR1, a MAD-related protein that functions in BMP2 signaling pathways, Cell 85 (1996) 489–500.
[9] T. Katagiri, T. Watabe, Bone morphogenetic proteins, Cold Spring Harb. Perspect. Biol. 8 (2016).
[10] R. Nishimura, Y. Kato, D. Chen, S.E. Harris, G.R. Mundy, T. Yoneda, Smad5 and DPC4 are key molecules in mediating BMP-2-induced osteoblastic differentiation of the pluripotent mesenchymal precursor cell line C2C12, J. Biol. Chem. 273 (1998) 1872–1879.

[11] Y. Shi, J. Massague, Mechanisms of TGF-beta signaling from cell membrane to the nucleus, Cell 113 (2003) 685–700.
[12] C.H. Heldin, A. Moustakas, Signaling receptors for TGF-beta family members, Cold Spring Harb. Perspect. Biol. 8 (2016).
[13] I.H. Ali, D.P. Brazil, Bone morphogenetic proteins and their antagonists: current and emerging clinical uses, Br. J. Pharmacol. 171 (2014) 3620–3632.
[14] J.K. Burkus, H.S. Sandhu, M.F. Gornet, M.C. Longley, Use of rhBMP-2 in combination with structural cortical allografts: clinical and radiographic outcomes in anterior lumbar spinal surgery, J. Bone Joint Surg. Am. 87 (2005) 1205–1212.
[15] K.S. Cahill, P.C. McCormick, A.D. Levi, A comprehensive assessment of the risk of bone morphogenetic protein use in spinal fusion surgery and postoperative cancer diagnosis, J. Neurosurg. Spine 23 (2015) 86–93.
[16] J.W. Lowery, D. Pazin, G. Intini, S. Kokabu, V. Chappuis, L.P. Capelo, V. Rosen, The role of BMP2 signaling in the skeleton, Crit. Rev. Eukaryot. Gene Expr. 21 (2011) 177–185.
[17] A.H. Simpson, L. Mills, B. Noble, The role of growth factors and related agents in accelerating fracture healing, J. Bone Joint Surg. Br. 88 (2006) 701–705.
[18] A.P. White, A.R. Vaccaro, J.A. Hall, P.G. Whang, B.C. Friel, M.D. McKee, Clinical applications of BMP-7/OP-1 in fractures, nonunions and spinal fusion, Int. Orthop. 31 (2007) 735–741.
[19] N.Y. Yu, A. Schindeler, M. Tagil, A.J. Ruys, D.G. Little, Use of BMPs and bisphosphonates in improving bone fracture healing, Front. Biosci. (Elite Ed) 4 (2012) 2647–2653.
[20] J.W. Lowery, V. Rosen, Bone morphogenetic protein-based therapeutic approaches, Cold Spring Harb. Perspect. Biol. 10 (2018).
[21] N. Kamiya, T. Kobayashi, Y. Mochida, P.B. Yu, M. Yamauchi, H.M. Kronenberg, Y. Mishina, Wnt inhibitors Dkk1 and Sost are downstream targets of BMP signaling through the type IA receptor (BMPRIA) in osteoblasts, J. Bone Miner. Res. 25 (2010) 200–210.
[22] N. Kamiya, L. Ye, T. Kobayashi, D.J. Lucas, Y. Mochida, M. Yamauchi, H.M. Kronenberg, J.Q. Feng, Y. Mishina, Disruption of BMP signaling in osteoblasts through type IA receptor (BMPRIA) increases bone mass, J. Bone Miner. Res. 23 (2008) 2007–2017.
[23] N. Kamiya, L. Ye, T. Kobayashi, Y. Mochida, M. Yamauchi, H.M. Kronenberg, J.Q. Feng, Y. Mishina, BMP signaling negatively regulates bone mass through sclerostin by inhibiting the canonical Wnt pathway, Development 135 (2008) 3801–3811.
[24] Y. Mishina, M.W. Starbuck, M.A. Gentile, T. Fukuda, V. Kasparcova, J.G. Seedor, M.C. Hanks, M. Amling, G.J. Pinero, S. Harada, et al., Bone morphogenetic protein type IA receptor signaling regulates postnatal osteoblast function and bone remodeling, J. Biol. Chem. 279 (2004) 27560–27566.
[25] N. Kamiya, L. Shuxian, R. Yamaguchi, M. Phipps, O. Aruwajoye, N.S. Adapala, H. Yuan, H.K. Kim, J.Q. Feng, Targeted disruption of BMP signaling through type IA receptor (BMPR1A) in osteocyte suppresses SOST and RANKL, leading to dramatic increase in bone mass, bone mineral density and mechanical strength, Bone 91 (2016) 53–63.
[26] J. Lim, Y. Shi, C.M. Karner, S.Y. Lee, W.C. Lee, G. He, F. Long, Dual function of Bmpr1a signaling in restricting preosteoblast proliferation and stimulating osteoblast activity in mouse, Development 143 (2016) 339–347.
[27] N. Kamiya, V.M. Kaartinen, Y. Mishina, Loss-of-function of ACVR1 in osteoblasts increases bone mass and activates canonical Wnt signaling through suppression of Wnt inhibitors SOST and DKK1, Biochem. Biophys. Res. Commun. 414 (2011) 326–330.
[28] J.W. Lowery, G. Intini, L. Gamer, S. Lotinun, V.S. Salazar, S. Ote, K. Cox, R. Baron, V. Rosen, Loss of BMPR2 leads to high bone mass due to increased osteoblast activity, J. Cell Sci. 128 (2015) 1308–1315.
[29] M. Baud'huin, N. Solban, M. Cornwall-Brady, D. Sako, Y. Kawamoto, K. Liharska, D. Lath, M.L. Bouxsein, K.W. Underwood, J. Ucran, et al., A soluble bone morphogenetic protein type IA receptor increases bone mass and bone strength, Proc. Natl. Acad. Sci. U. S. A. 109 (2012) 12207–12212.
[30] Y. Zhang, E.G. McNerny, M. Terajima, M. Raghavan, G. Romanowicz, Z. Zhang, H. Zhang, N. Kamiya, M. Tantillo, P. Zhu, et al., Loss of BMP signaling through BMPR1A in osteoblasts leads to greater collagen cross-link maturation and material-level mechanical properties in mouse femoral trabecular compartments, Bone 88 (2016) 74–84.
[31] A. Iura, E.G. McNerny, Y. Zhang, N. Kamiya, M. Tantillo, M. Lynch, D.H. Kohn, Y. Mishina, Mechanical loading synergistically increases trabecular bone volume and improves mechanical properties in the mouse when BMP signaling is specifically ablated in osteoblasts, PLoS One 10 (2015) e0141345.
[32] E. Barrett-Connor, C.M. Nielson, E. Orwoll, D.C. Bauer, J.A. Cauley, Osteoporotic Fractures in Men Study G, Epidemiology of rib fractures in older men: osteoporotic fractures in men (MrOS) prospective cohort study, BMJ 340 (2010) c1069.
[33] J. Duan, Y. Lee, C. Jania, J. Gong, M. Rojas, L. Burk, M. Willis, J. Homeister, S. Tilley, J. Rubin, et al., Rib fractures and death from deletion of osteoblast beta-catenin in adult mice is rescued by corticosteroids, PLoS One 8 (2013) e55757.
[34] L.A. Wuermser, S.J. Achenbach, S. Amin, S. Khosla, L.J. Melton 3rd, What accounts for rib fractures in older adults? J. Osteoporos. 2011 (2011) 457591.
[35] B.C. Carlson, W.A. Robinson, N.R. Wanderman, A.S. Sebastian, A. Nassr, B.A. Freedman, P.A. Anderson, A review and clinical perspective of the impact of osteoporosis on the spine, Geriatr. Orthop. Surg. Rehabil. 10 (2019) 2151459319861591.
[36] M.L. Gourlay, R.A. Overman, J.P. Fine, G. Filteau, P.M. Cawthon, J.T. Schousboe, E.S. Orwoll, T.J. Wilt, T.V. Nguyen, N.E. Lane, et al., Time to osteoporosis and major fracture in older men: the MrOS study, Am. J. Prev. Med. 50 (2016) 727–736.
[37] T. Kobayashi, M. Kaneko, M. Narukawa, Influence of prevalent vertebral fracture on the correlation between change in lumbar spine bone mineral density and risk of new vertebral fracture: a meta-analysis of randomized clinical trials, Clin. Drug Investig. 40 (2020) 15–23.
[38] J. Rossert, H. Eberspaecher, B. de Crombrugghe, Separate cis-acting DNA elements of the mouse pro-alpha 1(I) collagen promoter direct expression of reporter genes to different type I collagen-producing cells in transgenic mice, J. Cell Biol. 129 (1995) 1421–1432.
[39] Y. Mishina, M.C. Hanks, S. Miura, M.D. Tallquist, R.R. Behringer, Generation of Bmpr/Alk3 conditional knockout mice, Genesis 32 (2002) 69–72.
[40] M. Yamauchi, Y. Taga, S. Hattori, M. Shiiba, M. Terajima, Analysis of collagen and elastin cross-links, Methods Cell Biol. 143 (2018) 115–132.
[41] M. Katafuchi, T. Matsuura, P. Atsawasuwan, H. Sato, M. Yamauchi, Biochemical characterization of collagen in alveolar mucosa and attached gingiva of pig, Connect. Tissue Res. 48 (2007) 85–92.
[42] M. Sricholpech, I. Perdivara, M. Yokoyama, H. Nagaoka, M. Terajima, K.B. Tomer, M. Yamauchi, Lysyl hydroxylase 3-mediated glucosylation in type I collagen: molecular loci and biological significance, J. Biol. Chem. 287 (2012) 22998–23009.
[43] M. Terajima, I. Perdivara, M. Sricholpech, Y. Deguchi, N. Pleshko, K.B. Tomer, M. Yamauchi, Glycosylation and cross-linking in bone type I collagen, J. Biol. Chem. 289 (2014) 22636–22647.
[44] A. Carden, R.M. Rajachar, M.D. Morris, D.H. Kohn, Ultrastructural changes accompanying the mechanical deformation of bone tissue: a Raman imaging study, Calcif. Tissue Int. 72 (2003) 166–175.
[45] J.M. Wallace, K. Golcuk, M.D. Morris, D.H. Kohn, Inbred strain-specific response to biglycan deficiency in the cortical bone of C57BL6/129 and C3H/He mice, J. Bone Miner. Res. 24 (2009) 1002–1012.
[46] E.P. Paschalis, K. Verdelis, S.B. Doty, A.L. Boskey, R. Mendelsohn, M. Yamauchi, Spectroscopic characterization of collagen cross-links in bone, J. Bone Miner. Res. 16 (2001) 1821–1828.
[47] K.J. Livak, T.D. Schmittgen, Analysis of relative gene expression data using real-time quantitative PCR and the 2(−Delta Delta C(T)) method, Methods 25 (2001) 402–408.
[48] W.C. Oliver, G.M. Pharr, An improved technique for determining hardness and elastic modulus using load and displacement sensing indentation experiments, J. Mater. Res. 7 (1992) 1564–1583.
[49] K.J. Jepsen, S.A. Goldstein, J.L. Kuhn, M.B. Schaffler, J. Bonadio, Type-I collagen mutation compromises the post-yield behavior of Mov13 long bone, J. Orthop. Res. 14 (1996) 493–499.
[50] G.M. Reeves, B.R. McCreadie, S. Chen, A.T. Galecki, D.T. Burke, R.A. Miller, S.A. Goldstein, Quantitative trait loci modulate vertebral morphology and mechanical properties in a population of 18-month-old genetically heterogeneous mice, Bone 40 (2007) 433–443.
[51] M. Saito, K. Fujii, K. Marumo, Degree of mineralization-related collagen cross-linking in the femoral neck cancellous bone in cases of hip fracture and controls, Calcif. Tissue Int. 79 (2006) 160–168.
[52] M. Yamauchi, M. Sricholpech, Lysine post-translational modifications of collagen, Essays Biochem. 52 (2012) 113–133.
[53] C. Shi, G.S. Mandair, H. Zhang, G.G. Vanrenterghem, R. Ridella, A. Takahashi, Y. Zhang, D.H. Kohn, M.D. Morris, Y. Mishina, et al., Bone morphogenetic protein signaling through ACVR1 and BMPR1A negatively regulates bone mass along with alterations in bone composition, J. Struct. Biol. 201 (2018) 237–246.
[54] E.P. Paschalis, E. Shane, G. Lyritis, G. Skarantavos, R. Mendelsohn, A.L. Boskey, Bone fragility and collagen cross-links, J. Bone Miner. Res. 19 (2004) 2000–2004.
[55] K.H. Larsen, C.M. Frederiksen, J.S. Burns, B.M. Abdallah, M. Kassem, Identifying a molecular phenotype for bone marrow stromal cells with in vivo bone-forming capacity, J. Bone Miner. Res. 25 (2010) 796–808.
[56] P.C. Trackman, Enzymatic and non-enzymatic functions of the lysyl oxidase family in bone, Matrix Biol. 52–54 (2016) 7–18.
[57] A. Wojtowicz, A. Dziedzic-Goclawska, A. Kaminski, W. Stachowicz, K. Wojtowicz, S.C. Marks Jr., M. Yamauchi, Alteration of mineral crystallinity and collagen cross-linking of bones in osteopetrotic toothless (tl/tl) rats and their improvement after treatment with colony stimulating factor-1, Bone 20 (1997) 127–132.
[58] T. Matsuura, K. Tokutomi, M. Sasaki, M. Katafuchi, E. Mizumachi, H. Sato, Distinct characteristics of mandibular bone collagen relative to long bone collagen: relevance to clinical dentistry, Biomed. Res. Int. 2014 (2014) 769414.
[59] T. van den Bos, D. Speijer, R.A. Bank, D. Bromme, V. Everts, Differences in matrix composition between calvaria and long bone in mice suggest differences in biomechanical properties and resorption: special emphasis on collagen, Bone 43 (2008) 459–468.
[60] D. Chalhoub, E.S. Orwoll, P.M. Cawthon, K.E. Ensrud, R. Boudreau, S. Greenspan, A.B. Newman, J. Zmuda, D. Bauer, S. Cummings, et al., Areal and volumetric bone mineral density and risk of multiple types of fracture in older men, Bone 92 (2016) 100–106.
[61] Y. Zhang, Y. Li, Q. Gao, B. Shao, J. Xiao, H. Zhou, Q. Niu, M. Shen, B. Liu, K. Hu, et al., The variation of cancellous bones at lumbar vertebra, femoral neck, mandibular angle and rib in ovariectomized sheep, Arch. Oral Biol. 59 (2014) 663–669.
[62] A.L. Mikula, R.C. Puffer, J.D.S. Jeor, J.T. Bernatz, J.L. Fogelson, A.N. Larson, A. Nassr, A.S. Sebastian, B.A. Freedman, B.L. Currier, et al., Teriparatide treatment increases Hounsfield units in the lumbar spine out of proportion to DEXA changes, J. Neurosurg. Spine (2019) 1–6.
[63] R. Hou, S.A. Cole, M. Graff, K. Haack, S. Laston, A.G. Comuzzie, N.R. Mehta, K. Ryan, D.L. Cousminer, B.S. Zemel, et al., Genetic variants affecting bone mineral density and bone mineral content at multiple skeletal sites in Hispanic children, Bone 132 (2020) 115175.
[64] D.M. Cullinane, K.T. Salisbury, Y. Alkhiary, S. Eisenberg, L. Gerstenfeld, T.A. Einhorn, Effects of the local mechanical environment on vertebrate tissue differentiation during repair: does repair recapitulate development, J. Exp. Biol.

206 (2003) 2459–2471.
[65] T.N. Gardner, T. Stoll, L. Marks, S. Mishra, M. Knothe Tate, The influence of mechanical stimulus on the pattern of tissue differentiation in a long bone fracture–an FEM study, J. Biomech. 33 (2000) 415–425.
[66] E.G. Loboa, G.S. Beaupre, D.R. Carter, Mechanobiology of initial pseudarthrosis formation with oblique fractures, J. Orthop. Res. 19 (2001) 1067–1072.
[67] X. Jiang, S. Iseki, R.E. Maxson, H.M. Sucov, G.M. Morriss-Kay, Tissue origins and interactions in the mammalian skull vault, Dev. Biol. 241 (2002) 106–116.
[68] D.M. Noden, P.A. Trainor, Relations and interactions between cranial mesoderm and neural crest populations, J. Anat. 207 (2005) 575–601.
[69] B. Behr, N.J. Panetta, M.T. Longaker, N. Quarto, Different endogenous threshold levels of fibroblast growth factor-ligands determine the healing potential of frontal and parietal bones, Bone 47 (2010) 281–294.
[70] J. Liu, H.K. Nam, E. Wang, N.E. Hatch, Further analysis of the Crouzon mouse: effects of the FGFR2(C342Y) mutation are cranial bone-dependent, Calcif. Tissue Int. 92 (2013) 451–466.
[71] C.S. Yee, J.O. Manilay, J.C. Chang, N.R. Hum, D.K. Murugesh, J. Bajwa, M.E. Mendez, A.E. Economides, D.J. Horan, A.G. Robling, et al., Conditional deletion of Sost in MSC-derived lineages identifies specific cell-type contributions to bone mass and B-cell development, J. Bone Miner. Res. 33 (2018) 1748–1759.